

## Low Symmetric *meso*–Borneol and *meso*–Carbazole Substituted $H_3$ Corroles: Synthesis, Characterization and Their Anticancer Behaviors

Rongping Tang,<sup>a</sup> Zhouqun Ji,<sup>b</sup> Lin Xie,<sup>a</sup> Hongyan Lu,<sup>b</sup> Wei Tang,<sup>b@1</sup> and Xu Liang<sup>a,c@2</sup>

<sup>a</sup>Lanzhou Petrochemical College of Vocational Technology, Lanzhou 730050, P. R. China

<sup>b</sup>Department of Pediatrics, Affiliated Hospital of Jiangsu University, Zhenjiang 210000, P. R. China

<sup>c</sup>School of Chemistry and Chemical Engineering, Jiangsu University, Zhenjiang 212013, P. R. China

@<sup>1</sup>Corresponding author E-mail: zjtangwei@163.com

@<sup>2</sup>Corresponding author E-mail: liangxu@ujs.edu.cn

*Two  $A_2B$  type free base corroles with meso-borneol substituents at the B position have been synthesized and characterized. A detailed analysis of the optical and redox properties was carried out, and a comparison was made with theoretical calculations to identify the key trends in the structure-property relationships. The meso-borneol substituent couples strongly with the porphyrin core leading to significant CD signals in the B band region. Enhanced anti-cancer properties are observed in vitro relative to the introduction of (–)-borneol units.*

**Keywords:** Corrole, borneol, molecular chirality, photophysics, anticancer behavior.

## Низкосимметричные мезо–борнеол и мезо–карбазол–замещенные $H_3$ –корролы: синтез, характеристика, противораковое действие

Жунпин Тан,<sup>a</sup> Чжоу Цзи,<sup>b</sup> Линь Се,<sup>a</sup> Хунъян Лу,<sup>b</sup> Вэй Тан,<sup>b@1</sup> Сюй Лян<sup>a,c@2</sup>

<sup>a</sup>Ланьчжоуский нефтехимический колледж профессиональных технологий, Ланьчжоу 730050, КНР

<sup>b</sup>Кафедра педиатрии, Больница при университете Цзянсу, Чжэньцзян 210000, КНР

<sup>c</sup>Школа химии и химической инженерии, Университет Цзянсу, Чжэньцзян 212013, КНР

@<sup>1</sup>E-mail: zjtangwei@163.com

@<sup>2</sup>E-mail: liangxu@ujs.edu.cn

*На основе свободного основания с мезо-борнеольными заместителями в положении В синтезированы и охарактеризованы два коррола типа  $A_2B$ . Был проведен подробный анализ оптических и окислительно-восстановительных свойств, а также проведено сравнение с теоретическими расчетами для выявления ключевых тенденций во взаимосвязях структура-свойство. Мезо-борнеольная группа прочно соединяется с порфириновым ядром, что приводит к появлению значительных сигналов в спектре кругового дихроизма в области В-полосы. При введении фрагментов (–)-борнеола наблюдается усиление противоракового эффекта in vitro.*

**Ключевые слова:** Коррол, борнеол, хиральность молекул, фотофизика, противораковые свойства.

## Introduction

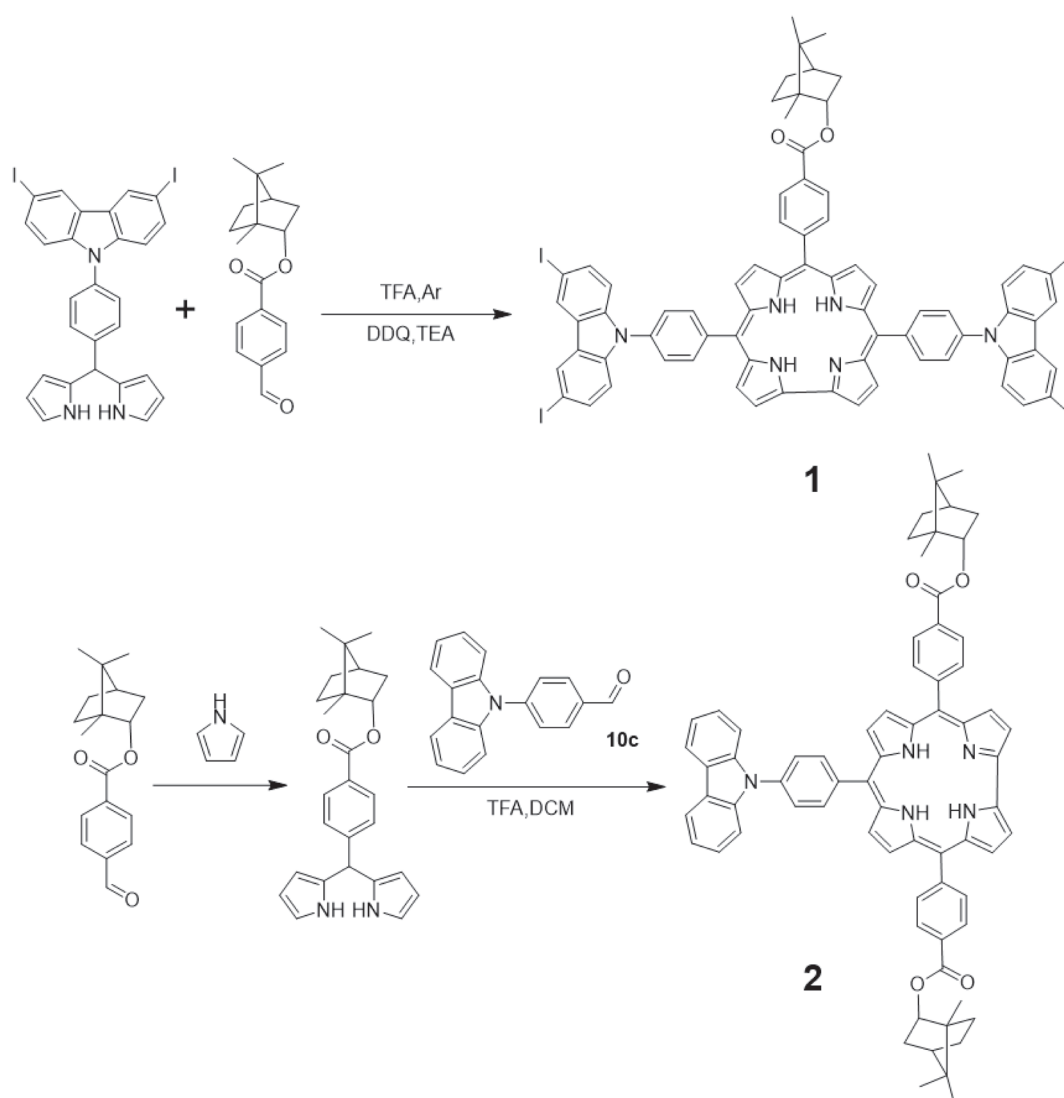
Porphyrins, a group of highly conjugated heterocyclic macrocycle organic compounds, composed of four modified pyrrole subunits interconnected at their  $\alpha$  carbon atoms have been investigated in various fields during past decades.<sup>[1–4]</sup> Corroles are important porphyrin derivatives that provide sterically constrained environments for coordinating central cations, since in contrast with porphyrins they have three inner N–H protons to maintain the heteroaromatic properties of the ligand  $\pi$ -system in the presence of only three *meso*-carbons.<sup>[5–7]</sup> Various functional groups can be introduced at the *meso*-,  $\beta$ -, and/or axial positions to modify the structures of the corrole ligands and their metal complexes.<sup>[8–10]</sup> Borneol, a bicyclic chiral monoterpene, is found in the essential oils of medicinal plants and is commonly used in traditional Chinese medicine for analgesia and anesthesia.<sup>[11–12]</sup> Borneol derivatives have been intensively studied in the field of medicinal, food and material chemistry.<sup>[13–14]</sup> Although research on borneol has led to a significantly enhanced understanding of its properties during the past few decades, the rational design of borneol derivatives to efficiently

enhance their properties is still a challenge.<sup>[15–17]</sup> Corroles can play an important role in various cancer therapies due to their biocompatibility and low biological toxicity.<sup>[18–20]</sup> Thus, we anticipate that borneol-substituted corroles may play an effective role in enhancing anti-cancer behavior, since the chiral borneol substituent can provide strong excitation coupling with the main spectral bands of the corrole ligand and hence can provide tunable molecular chiral-optical properties. In this study, the synthesis and characterization of a series of low symmetry A<sub>2</sub>B type corroles is reported, and their chiral-optical properties are investigated along with their anti-cancer properties.

## Experimental

### General

<sup>1</sup>H NMR spectra were recorded on a Bruker AVANCE III 600M spectrometer. Chemical shifts for <sup>1</sup>H NMR spectra were expressed in parts per million (ppm) relative to CDCl<sub>3</sub> ( $\delta$  = 7.26 ppm) as the internal standard. UV-Vis spectra were recorded on Shimadzu UV-2600 spectrophotometer at ambient temperature with



**Scheme 1.** Synthesis of low symmetric *meso*-borneol and *meso*-carbazole H<sub>3</sub>-corroles.

a 1 cm quartz cell. CD spectra were performed on a JASCO-810 spectrometer. Elemental analyses for C, H and N were performed on a Perkin Elmer 240C elemental analyzer. The High Resolution Mass Spectra (HRMS) data was performed on a LTQ Orbitrap XL spectrometer equipped with an electrospray ionization (ESI) source. Cyclic voltammetry was performed with a three-electrode-compartment cell in *o*-dichlorobenzene (*o*-DCB) solutions with 0.1 M [n-Bu<sub>4</sub>N](ClO<sub>4</sub>) as supporting electrolyte using CHI-730D electrochemistry workstation. A glassy carbon electrode of 3 mm diameter was used as the working electrode while platinum wire and Ag/AgCl electrodes were used as the counter and reference electrodes respectively. All electrochemical characterizations were measured under N<sub>2</sub> atmosphere.

## Synthesis

**5-(4-(3,6-Diiodo-9-(4-*N*-benzoylphenyl))carbazole)phenyl)dipyrromethane.** The freshly distilled pyrrole (50 mL, 704.00 mmol, excess amount) and trifluoroacetic acid (0.21 mL, 0.28 mmol) were dissolved in 100 mL of dry CH<sub>2</sub>Cl<sub>2</sub>, and 3,6-iodo-9-(4-*N*-benzoylphenyl)carbazole (0.71 g, 1.84 mmol) was slowly added over 1 h. After reaction was quenched by NaOH, the excess amount of pyrrole was fully removed by washing, extracting, and distilling. The target compound was finally obtained through silica gel column chromatography (CH<sub>2</sub>Cl<sub>2</sub>) to give the pure yellow solid state compound in a 87.6 % yield. <sup>1</sup>H NMR (600 MHz, CDCl<sub>3</sub>) δ ppm: 8.38 (d, *J* = 1.8 Hz, 2H), 8.04 (s, 2H), 7.65 (d, *J* = 9.0 Hz, 2H), 7.45–7.41 (m, 4H), 7.16 (d, *J* = 8.4 Hz, 2H), 6.78 (s, 2H), 6.22 (s, 2H), 5.99 (s, 2H), 5.60 (s, 1H).

**5,15-Bis(4-(3,6-diiodo-9-(4-*N*-benzoylphenyl))carbazole)phenyl)-10-(bornylhydroxybenzoate)corrole, **1**.** *p*-(Bornyl hydroxybenzoate)aldehyde (0.38 g, 0.94 mmol) and 5-(4-(3,6-diiodo-9-(4-*N*-benzoylphenyl))carbazole)phenyl)dipyrromethane (1.79 g, 2.80 mmol) were dissolved in 70 mL of CH<sub>2</sub>Cl<sub>2</sub> in the absence of light under Ar, and TFA (0.002 mL) was slowly added into the same solution. After the mixture was stirred about 4 h, DDQ (0.86 g, 3.80 mmol) was added, and the mixture was further reacted for 0.5 h. After organic solvent was removed, purification was passed by silica gel column chromatography (CH<sub>2</sub>Cl<sub>2</sub>:hexane = 3:2, v:v) and recrystallization (CHCl<sub>3</sub>/MeOH) to give the pure purple solid state compound in a 5.4 % yield. High-resolution-ESI-mass spectra: *m/z* = 1541.0368 (Calcd. for C<sub>72</sub>H<sub>53</sub>I<sub>4</sub>N<sub>6</sub>O<sub>2</sub> [M+H]<sup>+</sup> = 1541.0330). <sup>1</sup>H NMR (600 MHz, CDCl<sub>3</sub>) δ ppm: 9.08 (s, 4H), 8.78 (d, *J* = 11.4 Hz, 2H), 8.68–8.46 (m, 8H), 8.34–8.16 (m, 6H), 8.06 (d, *J* = 3.6 Hz, 4H), 7.76 (d, *J* = 3.6 Hz, 4H), 7.63 (d, *J* = 5.4 Hz, 4H), 5.34–5.31 (m, 1H), 2.64–2.61 (m, 1H), 2.34–2.31 (m, 1H), 1.92–1.87 (m, 1H), 1.85 (t, *J* = 4.2 Hz, 1H), 1.45–1.42 (m, 2H), 1.31–1.29 (m, 1H), 1.06 (s, 6H), 0.99 (s, 3H). Elemental analysis: C (56.22 %), H (3.52 %), N (5.36 %), O (2.01 %) (Calcd. for C<sub>72</sub>H<sub>52</sub>I<sub>4</sub>N<sub>6</sub>O<sub>2</sub> C, 56.12 %; H, 3.40 %; N, 5.45 %; O, 2.08 %). UV-Vis (CH<sub>2</sub>Cl<sub>2</sub>) λ<sub>max</sub> (nm) (ε·10<sup>-5</sup> L·mol<sup>-1</sup>·cm<sup>-1</sup>): 436 (1.421), 552 (0.112), 590 (0.101), 647 (0.131).

**5,15-(Bornyl hydroxybenzoate)-10-(4-(9-(4-*N*-benzoylphenyl))carbazole)phenyl)corrole, **2**.** The general synthetic procedure is similar with that of **1**, and the target compound was finally isolated as the purple solid state compound in a 7.2 % yield. High-resolution-ESI-mass spectra: *m/z* = 1552.5327 (Calcd. for C<sub>71</sub>H<sub>66</sub>N<sub>5</sub>O<sub>4</sub> [M+H]<sup>+</sup> = 1052.5037). <sup>1</sup>H NMR (600 MHz, CDCl<sub>3</sub>) δ ppm: 8.98–8.83 (m, 4H), 8.75 (s, 2H), 8.58–8.51 (m, 11H), 8.25 (d, *J* = 6.6 Hz, 2H), 8.05–7.98 (m, 2H), 7.88–7.84 (m, 2H), 7.58–7.55 (m, 3H), 7.44–7.42 (m, 2H), 5.31–5.29 (m, 2H), 2.67–2.61 (m, 2H), 2.35–2.32 (m, 2H), 1.92–1.88 (m, 2H), 1.84 (t, *J* = 4.2 Hz, 2H), 1.51–1.45 (m, 4H), 1.31–1.26 (m, 2H), 1.07 (s, 12H), 0.99 (s, 6H); Elemental analysis: C (81.12 %), H (6.32 %), N (6.60 %), O (6.01 %) (Calcd. for C<sub>71</sub>H<sub>65</sub>N<sub>5</sub>O<sub>4</sub> C, 81.04 %; H, 6.23 %; N, 6.66 %; O, 6.08 %). UV-Vis (CH<sub>2</sub>Cl<sub>2</sub>) λ<sub>max</sub> (nm) (ε·10<sup>-5</sup> L·mol<sup>-1</sup>·cm<sup>-1</sup>): 431 (0.692), 545 (0.088), 593 (0.101), 655 (0.131).

## Cell Viability Assays

The antitumor activities of the four compounds *in vitro* were evaluated by MTT assay against human hepatoma cells (HepG2). HepG2 cells were put in 96-well plates at a concentration of 1·10<sup>5</sup> cells/well, and incubated for 6 h. The cells in the wells were respectively treated with porphyrin compounds at various concentration for 68 h. Then, 20 μL MTT (4 mg/mL) was added to each well and incubated with cells for 4 h at 37 °C. After the supernatant was discarded, DMSO (200 μL) was added to each well and the absorbance were measured at 570 nm by use of a microplate scanning spectrophotometer to statistically measure cell viability.

## Results and Discussion

### Synthesis and Characterization

The synthesis of free base corroles **1** and **2** followed [2+1] synthetic procedures with *p*-(bornylhydroxybenzoate) aldehyde used as the key precursor. All solvents and reagents were carefully dried to ensure that the target molecules were obtained successfully. H<sub>3</sub>Corroles **1** and **2** were isolated in the moderate yields of 5.4 % and 7.2 %, respectively. This could be attributed to the low solubility and separation became much more difficult. The HR ESI-MS data for **1** and **2** contain an intense parent peaks at *m/z* = 1541.0368 (calcd. for C<sub>72</sub>H<sub>53</sub>I<sub>4</sub>N<sub>6</sub>O<sub>2</sub> [M+H]<sup>+</sup> = 1541.0330) and *m/z* = 1552.5327 (calcd. for C<sub>71</sub>H<sub>66</sub>N<sub>5</sub>O<sub>4</sub> [M+H]<sup>+</sup> = 1552.5037), respectively. This provides direct evidence that **1** and **2** were successfully synthesized. <sup>1</sup>H NMR spectra of **1** and **2** confirm the presence of the characteristic peaks for the bornyl-substituent between 1.0–3.0 and at *ca.* 5.2 ppm. The other proton peaks can be assigned to the β-protons of the corrole core and the *meso*-aryl substituents (Figure 1). On the other hand, these H<sub>3</sub>corroles were also fully confirmed by elemental analysis.

### Spectroscopic Properties

Spectroscopic characterizations were carried out to investigate trends in the electronic structure of **1** and **2**. The UV-visible absorption spectra in CH<sub>2</sub>Cl<sub>2</sub> are similar to those reported previously for 5,10,15-triphenylcorrole.<sup>[22–24]</sup> **1** with one borneol unit exhibits an intense *B* (or Soret) band absorption at *ca.* 424 nm, and three absorption *Q* bands at 577, 620 and 655 nm (Figure 2). Upon increasing the number of borneol units, the negligible changes were observed that indicated the mirror influence of *meso*-borneol and *meso*-carbazole units on the electronic structure. On the other hand, since the borneol moieties have the chiral centers, the excitation coupling between the *meso*-borneol-substituents and the corrole core was investigated by circular dichroism spectroscopy. In Figure 2 (bottom), +/- sign sequences are consistently observed in ascending energy terms in the *B* band region at *ca.* 423 nm. The points of intersection of the CD curve and *x*-axis correspond approximately to the *B* band maxima. Kobayashi and coworkers have demonstrated previously that the presence of peripheral substituents, such as binaphthyl rings, can result in enantiomers with significant CD intensity for the *B* and *Q* bands of the achiral porphyrinoid ligand with sign sequences that can be rationalized on the basis of well-defined molecular

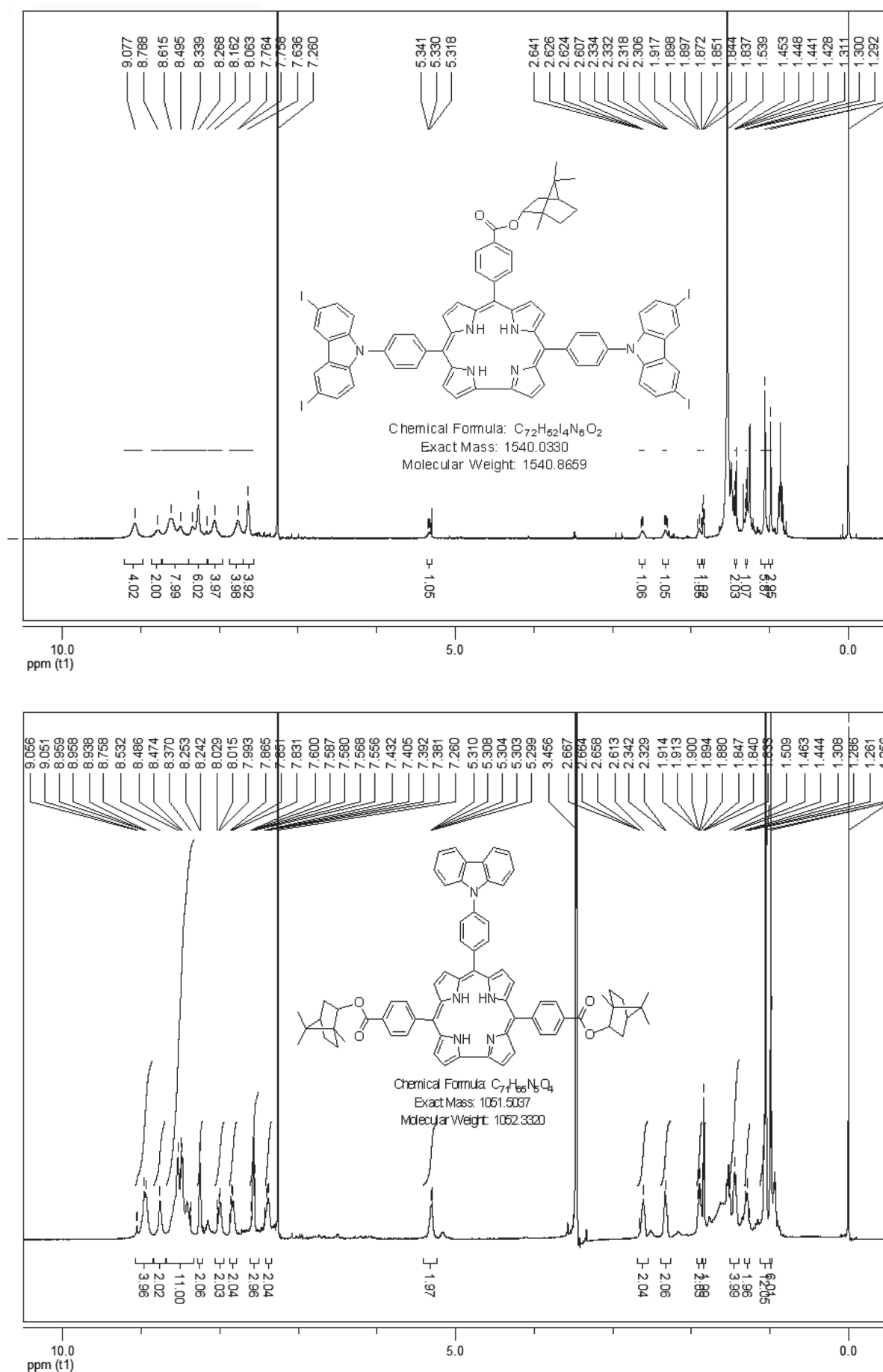
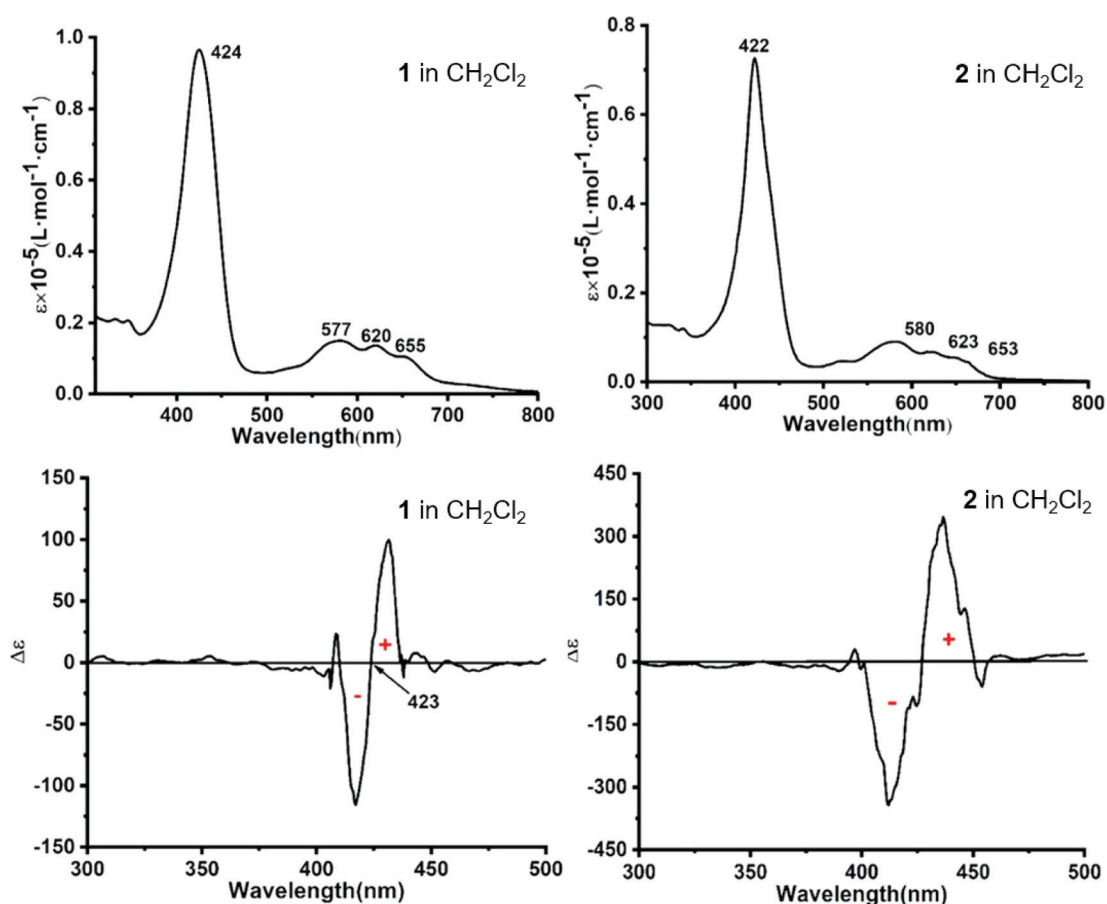


Figure 1. <sup>1</sup>H NMR spectra of **1** and **2** in CDCl<sub>3</sub> at 298 K.



**Figure 2.** UV-Vis absorption (top) and circular dichroism (CD, bottom) spectra of **1** and **2** in  $\text{CH}_2\text{Cl}_2$  at 298 K.

geometries through the Kuhn-Kirkwood coupled oscillator and/or “CD stealing” mechanisms.<sup>[21–23]</sup> In the context of this study, there is a scope for rotation of the A position *meso*-aryl ring, so, the relative orientations of the chiral substituent and the corrole core are not well defined.

### Electrochemistry

In order to gain insight into the perturbation of the electronic structures by the *meso*-borneol and *meso*-carbazole substituents, the energy levels of the HOMOs and LUMOs of **1** and **2** were checked by the electrochemical characterization methods cyclic voltammetry measurements (Figure 3), and all redox potentials were also derived from the half-sum of the potentials of the corresponding cathode and anode maxima.  $\text{H}_3\text{Corrole 1}$  has two-step reductions and oxidations which assigned as the 1<sup>st</sup> and 2<sup>nd</sup> steps ring oxidations and reductions, respectively. In addition,  $\text{H}_3\text{corrole 2}$  has only one ring of oxidation and reduction curves. The energy gap between the HOMO and the LUMO (H–L Gap) was also calculated from the dif-

ference between the electrochemical potentials of the 1<sup>st</sup> oxidation and 1<sup>st</sup> reduction (Table 1). The *ipRed* and *ipOx* values, determined from CV measurements for  $\text{H}_3\text{corroles 1}$  and **2** made at various scan-rates from 50–500 mV/s (Figure 3, bottom), provide an insight into the reversibility of the system on an experimental time-scale. The good linear correlations observed for plots of peak current vs.  $v^{1/2}$  for **1** and **2** confirm that all of the oxidation and reduction processes are diffusion controlled.

### Antitumor Activity Evaluation

The *in vitro* antitumor activities of the corrole derivatives **1** and **2** were evaluated against human cancer HepG2 cells by the MTT assay.  $\text{H}_3\text{Corrole 1}$  shows clear anticancer behavior, but it doesn't overcome 50 % (Figure 4). Upon increasing the number of borneol units,  $\text{H}_3\text{corrole 2}$  shows significant increase of the anticancer behavior, and the  $\text{IC}_{50}$  value of **2** is 73.63  $\mu\text{M}$ . As a conclusion, the compound **2** is expected to be developed as a potential antitumor agent through further study.

**Table 1.** Redox potentials (V) of  $\text{H}_3\text{corroles 1}$  and **2**.

Compound	$E_{1/2} \text{Ox}^{\text{II}}$	$E_{1/2} \text{Ox}^{\text{I}}$	$E_{1/2} \text{Red}^{\text{I}}$	$E_{1/2} \text{Red}^{\text{II}}$	H-L Gap
<b>1</b>	1.30	0.98	−1.51	−1.74	2.49
<b>2</b>	–	1.01	−1.49	–	2.50

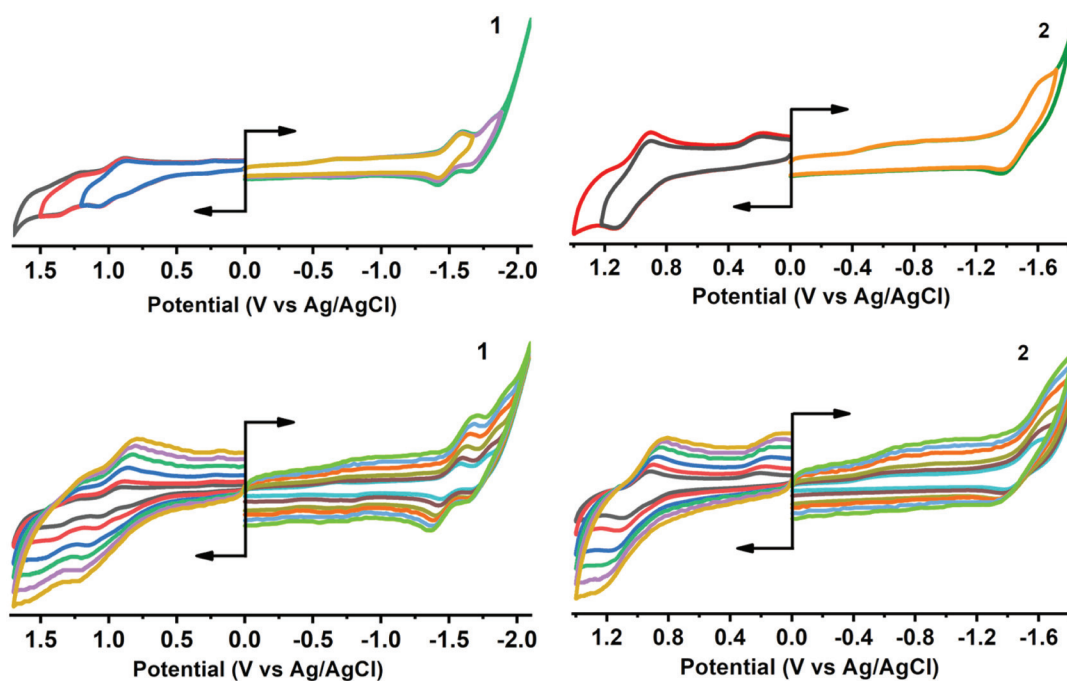


**Figure 3.** Cyclic voltammety measurements of H<sub>3</sub>corroles **1** and **2** (up, scan speed: 100 mV/s), CV measurement of H<sub>3</sub>corroles **1** and **2** at 50–500 mV/s scan speed (bottom) in *o*-dichlorobenzene containing 0.1M TBAP.

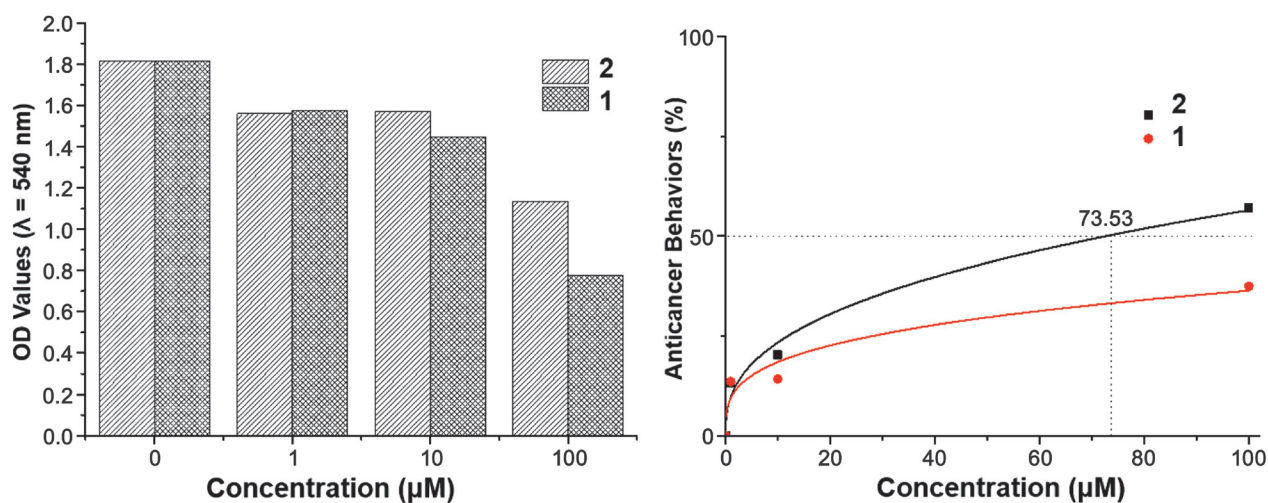


**Figure 4.** The influence of concentration (left) and the relationship of anticancer activity and concentration (right) of H<sub>3</sub>corroles **1** and **2**.

## Conclusions

Two A<sub>2</sub>B type free base corroles with borneol moieties introduced at the B positions have been successfully synthesized and characterized. A detailed analysis of the electronic structure was done through a comparison of the UV-visible absorption, circular dichroism and electrochemical characterizations. The results demonstrate that the A<sub>2</sub>B type borneol-substituted free base corroles provide multifunctional chromophores with novel chiral-optical responses and effective anti-tumor activities. Considering multifunctional chiral porphyrinoid chromophores have great potential for various applications,

these molecules could prove useful in biomedical applications.

**Acknowledgements.** This work was financially supported by the National Natural Science Foundation of China (21701058), the Key Laboratory of Functional Inorganic Material Chemistry (Heilongjiang University) of Ministry of Education, the China Post-doc Foundation (2018M642183), the Lanzhou High Talent Innovation and Entrepreneurship Project (2018-RC-105), Jiangsu University (17JDG035). We thank Prof. Dr. Haijun Xu from Nanjing Forestry University for sample measurements and fruitful discussions.

## References

1. Kaur R., Possanza F., Limosani F., Bauroth S., Zanoni R., Clark T., Arrigoni G., Tagliatesta P., Guldi D.M. *J. Am. Chem. Soc.* **2020**, *142*, 7898–7911.
2. Nurhayati, Suendo V., Alni A., Nugroho A.A., Majima Y., Lee S., Nugraha Y.P., Uekusa H. *J. Phys. Chem. A* **2020**, *124*, 2672–2682.
3. Zhu W.H., Haider S.N., Zhang H.L., Attatsi I.K., Mack J., Dingswayo S., Nyokong T., Song Y.T., Xu H.J., Liang X. *Dyes Pigment.* **2019**, *171*, 107740.
4. Liang X., Qiu Y.Y., Zhang X.F., Zhu W.H. *Dalton Trans.* **2020**, *49*, 3326–3332.
5. Ghosh A. *Chem. Rev.* **2017**, *117*, 3798–3881.
6. Barata J.F.B., Neves M.G.P.M.S., Faustino M.A.F., Tomé A.C., Cavaleiro J.A.S. *Chem. Rev.* **2017**, *117*, 3192–3253.
7. Orłowski R., Gryko D., Gryko D. *Chem. Rev.* **2017**, *117*, 3102–3137.
8. Liang X., Qiu Y.Y., Zhang X.F., Zhu W.H. *Dalton Trans.* **2020**, *49*, 3326–3332.
9. Berezina N.M., Vu Thi Thao, Berezin D.B., Bazanov M.I. *Russ. J. Inorg. Chem.* **2017**, *62*, 1619–1623.
10. Cai F.J., Xia F., Guo Y.X., Zhu W.H., Fu B., Liang X., Cai Z.C., Xu H.J. *New J. Chem.* **2019**, *43*, 18012–18017.
11. Khine A.A., Yang M.Y., Hu A.R., Lin G.H., Toh Y.H., Chen H.P. *Enzym. Microb. Technol.* **2020**, *139*, 109586.
12. Ying-Jiao L., Li-Juan X., Lan X., Li-Min G., Ta-Si L., Nai-Hong Ch. *Pharm. Chem. J.* **2020**, *54*, 154–161.
13. Rigano D., Formisano C., Rosselli S., Badalamenti N., Bruno M. *Nat. Prod. Commun.* **2020**, *15*, 1–7.
14. Singh A., Chopra H.K. *Tetrahedron: Asymmetry* **2016**, *27*, 448–453.
15. Darnell M., Weidolf L. *Chem. Res. Toxicol.* **2013**, *26*, 1139–1155.
16. van Osch D.J.G.P., Dietz C.H.J.T., Warrag S.E.E., Kroon M.C. *ACS Sustainable Chem. Eng.* **2020**, *8*, 10591–10612.
17. Liu H.L., Sun B.G. *J. Agric. Food. Chem.* **2018**, *66*, 5425–5432.
18. Teo R.D., Hwang J.Y., Termini J., Gross Z., Gray H.B. *Chem. Rev.* **2017**, *117*, 2711–2729.
19. Lim P., Mahammed A., Okun Z., Saltsman I., Gross Z., Gray H.B. *Chem. Res. Toxicol.* **2012**, *25*, 400–409.
20. Hwang J.Y., Lubow J., Chu D., Ma J., Agadjanian H., Sims J., Gray H.B., Gross Z., Farkas D.L. *Mol. Pharmaceutics* **2011**, *8*, 2233–2243.
21. Kobayashi N., Muranaka A., Mack J. *Circular Dichroism and Magnetic Circular Dichroism Spectroscopy for Organic Chemists*. Royal Society of Chemistry: Cambridge, **2011**.
22. Kobayashi N., Higashi R., Titeca B.C., Lamote F., Ceulemans A. *J. Am. Chem. Soc.* **1999**, *121*, 12018.
23. Muranaka A., Okuda M., Kobayashi N., Somer K., Ceulemans A. *J. Am. Chem. Soc.* **2004**, *126*, 4596–4604.

Received 15.09.2020

Accepted 16.12.2020